Hyperfine Interact
DOI 10.1007/s10751-013-0912-8

Annealing embrittlement of $Fe_{78}Si_9B_{13}$ (METGLAS-2605S2)

J. M. Cadogan · S. J. Campbell · J. Jing · C. P. Foley · P. Kater · Y. W. Mai

Abstract The ductile to brittle transition that occurs in amorphous $Fe_{78}Si_9B_{13}$ (METGLAS-2605S2) has been investigated using mechanical measurements over the temperature range 250–370 °C. The fracture toughness values, K_{Ic}, have been determined for a range of annealing times (5–30 min) and cooling rates of 15–45 °C/min. A pronounced ductile to brittle transition is observed around 310(10) °C although no obvious structural changes are evident as indicated by x-ray diffraction. Comparison of transmission and back-scattered conversion electron ^{57}Fe Mössbauer spectra for the bulk as-received ribbon in the ductile state ($K_{Ic} = 52$ MPa $\cdot \sqrt{m}$) and the ribbon annealed to the brittle state ($K_{Ic} \sim 10$ MPa $\cdot \sqrt{m}$) indicates magnetic texture effects in both the bulk and on the surface of these amorphous ribbons, related to the magnetostriction resulting from the quenched-in stress during the ribbon production process, and the ensuing stress-relief upon annealing.

Keywords Amorphous materials · Embrittlement · Mössbauer spectroscopy · Fracture toughness

Proceedings of the 32nd International Conference on the Applications of the Mössbauer Effect (ICAME 2013) held in Opatija, Croatia, 1–6 September 2013.

J. M. Cadogan (✉) · S. J. Campbell · J. Jing
School of Physical, Environmental and Mathematical Sciences,
UNSW Canberra at the Australian Defence Force Academy,
Canberra, BC 2610, Australia
e-mail: s.cadogan@adfa.edu.au

C. P. Foley
CSIRO Division of Materials Science and Engineering,
Bradfield Road, West Lindfield, NSW 2070, Australia

P. Kater · Y. W. Mai
Centre for Advanced Materials Technology, School of Aerospace,
Mechanical and Mechatronic Engineering J07,
The University of Sydney, Sydney, NSW 2006, Australia

Published online: 23 October 2013

1 Introduction

Amorphous Fe-Si-B alloys have been extensively studied over several decades. They exhibit a wide range of useful physical and structural properties, particularly their soft magnetic behaviour, and offer a range of useful electrical and electronic applications [1–3]. Annealing at temperatures well below the glass transition and crystallisation is essential for the enhancement of the soft magnetic properties of metallic glasses. In the case of commercially available $Fe_{78}Si_9B_{13}$ (METGLAS-2605S2) the manufacture recommended annealing at 365 °C for 3 h under an argon or nitrogen atmosphere in the presence of a magnetic field [4]. However, annealing below 400 °C is sufficient to cause embrittlement of the normally ductile material, creating difficulties for the subsequent application of these metallic glasses.

Numerous studies of the embrittlement of Fe-Si-B-type amorphous materials have been reported and it is clear that the mechanical properties of the metallic glasses are strongly dependent on the composition, e.g. [5–9]. Similarly, a wide range of factors are found to impact on the embrittlement and recovery processes in Fe-Si-B-type amorphous alloys. Small and Davies [5] demonstrated that extended pulverisation of embrittled ribbon led to at least partial recovery of malleability resulting from re-introduction of excess free volume. Sasaki et al. [6] concentrated on temperatures between 350–450 °C and developed an optimal annealing process for METGLAS-2605S2 with the aim of providing a significant improvement of the magnetic properties while minimising the deterioration of the mechanical properties. They found that annealing at 400 °C for 20 min in nitrogen could occur without creating significant structural relaxation and that structural relaxation is reflected in the embrittlement of the amorphous ribbons. A study of the effects of annealing Fe-Si-B using small-angle x-ray scattering and transmission electron microscopy [7] demonstrated that embrittlement proceeded predominantly as a two-stage process; the first stage is caused by topological short-range order with the second stage ascribed to compositional short-range order. Yamasaki et al. [7] noted that the susceptibility to first-stage embrittlement increased when the boron content exceeded 13 at.%. Scanning electron microscopy combined with electrical resistivity measurements indicated that annealing embrittlement in the Mo-doped metallic glass $(Fe_{0.99}Mo_{0.01})_{78}Si_9B_{13}$ was due to stress localisation resulting from the precipitation of nanoscale granular bcc α-Fe(Si,Mo) [10]. Niu et al. [8] have claimed that the embrittlement of Fe-Si-B glasses is caused by the precipitation of Fe-Si phases.

More recently, Cabral–Prieto et al. [11] investigated the effects of heat treatments in the range 23–490 °C using both triangular and saw-tooth heating and cooling rates. The microhardness measurements together with ^{57}Fe Mössbauer spectroscopy studies indicated, perhaps unsurprisingly, that the residual ductility of partially crystalline $Fe_{78}Si_9B_{13}$ depends markedly on the previous thermal history. Positron annihilation lifetime spectroscopy suggested that modifications occurred on both the surface and bulk of the ribbons. The more pronounced effects occurring on the surface were considered to be the main cause of the hardening of the amorphous alloy. Wu and Spaepen [12] explored the ductile to brittle transition in a $Fe_{79.3}Si_{4.0}B_{16.4}C_{0.3}$ glass by fracture bending strain measurements through the temperature region of embrittlement. They correlated the temperature shift in the ductile to brittle transition on isochronal annealing with the change in enthalpy due to structural relaxation. With the aid of a phenomenological model Wu and Spaepen [12] accounted for the

correlation based on the free-volume model for flow and a critical minimum value of the free volume for ductility.

^{57}Fe Mössbauer spectroscopy has been applied successfully in a number of investigations of effects related to the embrittlement of Fe-Si-B-type amorphous alloys, e.g. [11, 13, 14]. Comparisons of the spectral responses of a series of amorphous $Fe_{100-x-y}Si_yB_x$ alloys led Dubois et al. [13] to conclude that Fe and Si atoms are located in similar sites for $y \leq 9$ while the B atoms occupy interstitial sites with ∼9 Fe nearest-neighbour atoms. The re-crystallisation processes in Fe-Si-B were shown to differ from those of Fe-B alloys as metastable boride phases were not observed. Randrianantoandro et al. [14] carried out a detailed study of the re-crystallisation processes in $Fe_{78}Si_9B_{13}$ (METGLAS-2605S2) using ^{57}Fe Mössbauer spectroscopy in both transmission and back-scattering modes (conversion electron Mössbauer spectroscopy). This enabled them to explore the mechanisms responsible for crystallisation in the bulk material, and for both the shiny side (wheel contact and therefore more rapid quenching from the melt) and the dull side of the amorphous ribbon. The onset of surface crystallisation was found to occur simultaneously with the out-of-plane anisotropy and Randrianantoandro et al. [14] concluded that structural and chemical inhomogeneities induced during solidification account for differences in crystallisation between the shiny and dull surfaces.

The mechanisms underpinning the embrittlement process remain an open question and much recent work had focussed on plasticity ('Shear Transformation Zone') models [15–17]. Rycroft and Bouchbinder [18] recently published the results of their mathematical study of plastic deformation in glasses. The focus of that paper was on the fracture toughness, K_{Ic}, which is also one of the key parameters we have investigated in our study. The plastic deformation model gave quite good agreement with experimental values of K_{Ic} and holds the promise of providing at least a good qualitative understanding of this important mechanical behaviour.

Here, we present the outcome of an investigation of the embrittlement of $Fe_{78}Si_9B_{13}$ (METGLAS-2605S2) by fracture toughness and ^{57}Fe Mössbauer spectroscopy measurements. The ductile to brittle transition around 310(10) °C is reflected by pronounced changes in the fracture toughness on annealing at temperatures in the range ∼250–360 °C and this combined mechanical/Mössbauer approach serves to ensure that the samples we study here were in the optimally embrittled state. Transmission and conversion electron ^{57}Fe Mössbauer spectroscopy reveals magnetic textural effects for samples in both the ductile and brittle states.

2 Experimental methods

The amorphous METGLAS-2605S2 ribbons were supplied by Allied Chemical Co./METGLAS Inc. USA. The ribbons were heated in a nitrogen atmosphere at a rate of 120 °C/min to various temperatures in the range 250–360 °C, held at the maximum temperature for between 5 and 120 min and then cooled at rates of 15–45 °C/min. These temperatures are well below the crystallisation temperature of 540–565 °C and are similar to the temperatures recommended for magnetic annealing to enhance the commercial magnetic properties of these glassy metals.

X-ray diffraction was carried out on a Philips diffractometer using Cu-K_α radiation. Differential Scanning Calorimetry (DSC) was carried out on a Perkin-

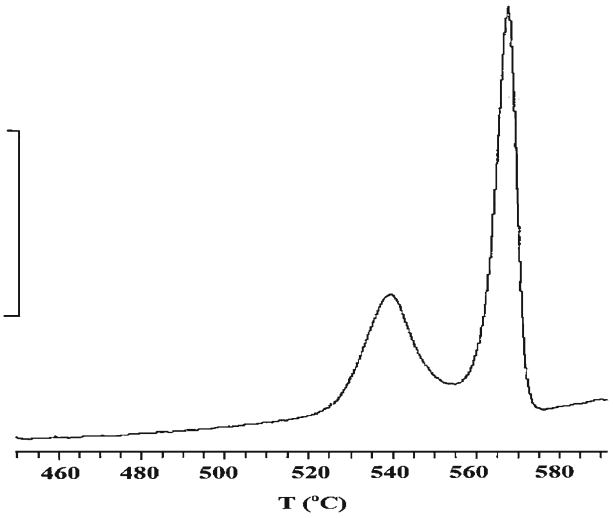

Fig. 1 DSC trace of the $Fe_{78}Si_9B_{13}$ sample after annealing at 360 °C for 5 min. The *vertical bar* represents a heat flow of 10 mW

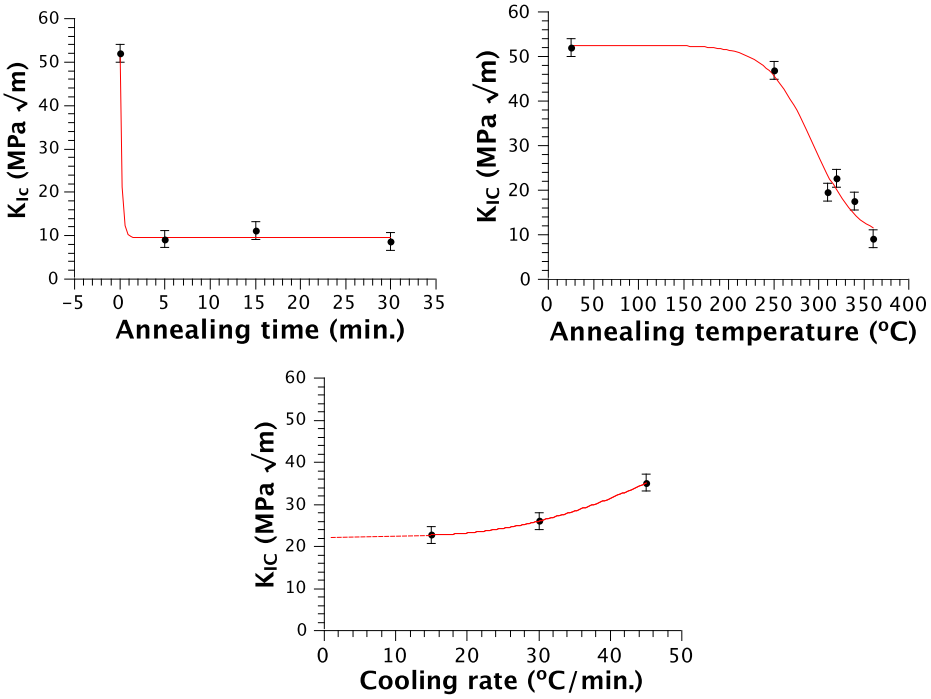

Fig. 2 Dependence of the METGLAS fracture toughness on: (*top left*) annealing time for the samples annealed at 360 °C, (*top right*) annealing temperature for 5 min anneals and (*bottom*) cooling rate for an annealing temperature of 320 °C. In the first two cases, the samples were cooled to RT at a rate of 15 °C/min. The *solid lines* are visual guides

Elmer system using a heating rate of 20 °C/min. The brittleness of our samples was characterised using the fracture toughness (K_{Ic}) which was determined by the standard 'single-edge notch test' method, using an Instron 4502 tensometer. Measurements were made on samples annealed between 250–370 °C with annealing times of 5–30 min and cooling rates of 15 °C/min.

^{57}Fe Mössbauer spectroscopy was carried out in both transmission and back-scattered conversion-electron modes using a 25 mCi ^{57}CoRh source on samples in the as-cast ductile state and in the annealed brittle state. The drive system was calibrated using α-Fe at room temperature and all spectra were fitted with a distribution of hyperfine fields, using the Le Caër-Dubois fitting program [19].

3 Results and discussion

3.1 Sample characterization

X-ray diffraction on both surfaces of the as-received samples confirmed the amorphous nature of the material. No signs of crystallinity were observed. This was also the case for the optimally embrittled samples reported here, confirming that the embrittled samples remain amorphous.

DSC shows that the crystallisation of both the as-received METGLAS-2605S2 sample in the ductile state and the annealed sample in the brittle state takes place as a two-stage process. The initial stage (see Fig. 1 for the DSC trace for the annealed sample in the brittle state) has a peak temperature of 539 °C corresponding to the precipitation of bcc α-Fe. The second stage has a peak temperature of 566 °C and represents the formation of crystalline Fe-B and Fe-Si phases [20]. The respective crystallisation temperatures for the embrittled sample are found to be the same as for the as-received sample, to within 2 °C. Interestingly, the heat associated with these crystallisation stages is smaller for the embrittled sample than for the ductile sample (by 2.7 and 6.1 %, respectively). This suggests that the embrittlement process could involve some development of a very short-range order similar to that proposed in the modelling of Fe-B amorphous materials in terms of Fe_3B-type short range order [21].

3.2 Fracture toughness

The as-received material is fully ductile and has $K_{Ic} = 52\ MPa \cdot \sqrt{m}$. The overall behaviour of the fracture toughness of $Fe_{78}Si_9B_{13}$ around the region of the embrittlement transition is shown in Fig. 2. In particular, the pronounced decrease in fracture toughness with temperature for an annealing time of 5 min is shown in the top right panel of Fig. 2. The transition from the ductile state to the brittle state is located around 310(10) °C. The rapidity with which the change from the ductile state to the brittle state occurs in $Fe_{78}Si_9B_{13}$ is evident from Fig. 2 (top left panel) in which the fracture toughness values change from $K_{Ic} \sim 50\ MPa \cdot \sqrt{m}$ to $K_{Ic} \sim 10\ MPa \cdot \sqrt{m}$, respectively, on annealing at 360 °C for approximately 1–2 min. The enhancement in K_{Ic} values for extended cooling rates on annealing at 320 °C as evident in Fig. 2 (bottom) indicates some weak recovery towards the ductile state of $Fe_{78}Si_9B_{13}$. This behaviour is likely to be associated with recovery towards the minimum free volume required for ductility, e.g. [12].

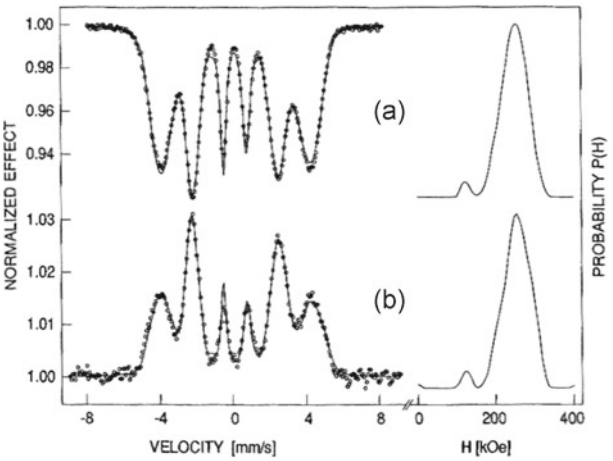

Fig. 3 ^{57}Fe Mössbauer transmission and CEMS spectra (obtained at 295 K) of the as-received $Fe_{78}Si_9B_{13}$ (METGLAS-2605S2) ribbon. The corresponding hyperfine field distributions are also shown

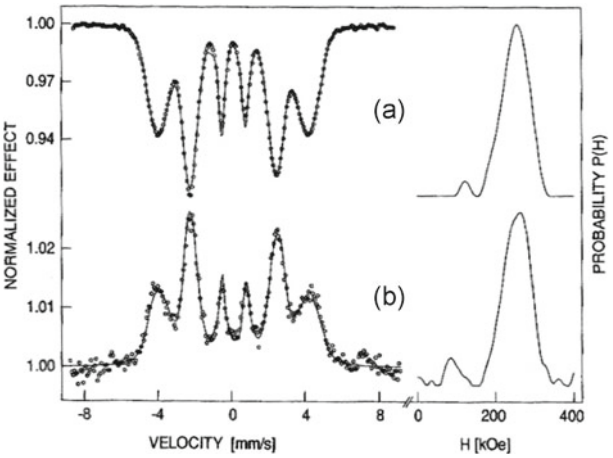

Fig. 4 ^{57}Fe Mössbauer transmission and CEMS spectra (obtained at 295 K) of $Fe_{78}Si_9B_{13}$ (METGLAS-2605S2) after embrittlement annealing at 360 °C for 5 min. The corresponding hyperfine field distributions are also shown

Table 1 ^{57}Fe Mössbauer data for $Fe_{78}Si_9B_{13}$ (METGLAS-2605S2)

The standard deviations of the hyperfine field distributions are denoted s.d.

Spectrum	Average hyperfine magnetic field (T)	*R*
As-received—bulk	24.8 (s.d. = 4.0)	2.2
As-received—surface	25.0 (s.d. = 4.3)	3.7
Annealed—bulk	24.8 (s.d. = 3.9)	2.8
Annealed—surface	24.1 (s.d. = 6.1)	4.0

3.3 Mössbauer spectroscopy

In Fig. 3 we show the transmission and CEMS ^{57}Fe Mössbauer spectra of the as-received $Fe_{78}Si_9B_{13}$ sample and in Fig. 4 we show the Mössbauer spectra of the sample annealed at 360 °C for 5 min, followed by cooling back to RT at a rate of 15 °C/min. As can be seen from Fig. 2 this sample has been annealed to the embrittled state and our XRD data confirmed that the sample is still amorphous. In Table 1 we summarise the average hyperfine fields and the magnetic texture parameter R (see below) for both samples.

The first thing to note is that no signs of crystallinity were observed on either side of the ribbons, either in the as-received state or after embrittlement annealing. The average ^{57}Fe hyperfine magnetic field in the bulk, as-received state is 24.8 T with a standard deviation of 4.0 T. The corresponding values for the ribbon surface in the as-received state are 25.0 T and 4.3 T. All spectra show some degree of magnetic texture, characterized by the relative intensities of lines 2 and 5 in the magnetic Mössbauer spectrum. We write the relative lines intensities in the standard form $3:R:1:1:R:3$ and the measured values of the texture parameter R are given in Table 1. The bulk as-received sample shows very little texture ($R = 2.2$) whereas the surface is highly textured ($R = 3.7$) with the moments lying close to the plane of the ribbon (i.e. perpendicular to the Mössbauer γ-ray direction). This is a common feature of melt-spun metallic glasses and is a consequence of the melt-spinning process.

The average ^{57}Fe hyperfine magnetic field in the bulk, annealed state is 24.8 T with a standard deviation of 3.9 T. The corresponding values for the ribbon surface in the annealed state are 24.1 T and 6.1 T. Therefore, the bulk material's hyperfine field is effectively unchanged by the embrittlement process. On the contrary, the surface shows a slight reduction in average hyperfine field with a sizable broadening of the hyperfine field distribution. A similar effect was observed in the transmission Mössbauer spectra of Fe-Ni-Mo-Si-B glasses by Škorvánek et al. [22] after prolonged annealing for several weeks. These authors attributed the broadening of the hyperfine field distribution to "*disturbances of the environment around iron caused by diffusion of constituent atoms during the annealing*". Our transmission spectra show no such broadening after short-term (up to 30 min) annealing.

The most significant difference between the as-received and embrittled samples is the increase in the magnetic texture along the ribbon plane in the bulk. The aforementioned line intensity ratio R in the bulk annealed sample is 2.8 (increased from 2.2). Magnetic texturing is a common feature of metallic glasses and the increase in texture upon embrittlement is most likely due to stress-relief caused by annealing. Such stress-relief has also been noted in resistivity measurements by Sasaki et al. [6]. The magnetic texture on the surface of the annealed ribbons is complete. The development of in-plane magnetic texture after structural relaxation is the result of competition between the (stress) induced anisotropy and the shape anisotropy. The local magnetization directions near the ribbon surface are under the strong influence of the demagnetization field which is a minimum when the magnetization is in-plane. The as-quenched ribbon is subject to substantial quenched-in residual stress and the large magnetostriction of Fe-based amorphous alloys may cause strong induced anisotropy (K_u) which supports the perpendicular component of surface magnetization [23–25].

4 Conclusions

We have studied the embrittlement of $Fe_{78}Si_9B_{13}$ (METGLAS-2605S2) using transmission and back-scattered CEMS Mössbauer spectroscopy and found evidence for magnetic texturing in both the bulk and on the surface of these amorphous ribbons. The degree of texture increases upon embrittlement annealing due to the concomitant structural relaxation. Measurements of the fracture toughness reveal a five-fold decrease in toughness around the ductile to brittle transition at 310(10) °C.

Acknowledgements We gratefully acknowledge support from the joint UNSW-CSIRO Research Fund. JMC is grateful to Prof. Kiyonori Suzuki (Monash University, Melbourne, Australia) for enlightening discussions.

References

1. Wolf, W., Mohs, R., Konig, U.: J. Magn. Magn. Mater. **19**, 177–82 (1980)
2. Herzer, G., Vazquez, M., Knobel, M., Zhukov, A., Reininger, T., Davies, H.A., Grössinger, R., Sanchez Ll., J.L.: J. Magn. Magn. Mater. **294**, 252–66 (2005)
3. Zhukov, A., González, J.: In: Liu, Y., Sellmayer, D.J., Shindo, D. (eds.) Handbook of Advanced Magnetic Materials, vol. 3, Chap. 5, pp. 115–181. Springer Science Publishers, New York. ISBN: 1-4020-7983-4 (2006)
4. Allied Chemical Corporation: METGLAS-2605S2, Product Information, USA (1988)
5. Small, C.J., Davies, H.A.: Mater. Sci. Eng. **97**, 457–60 (1988)
6. Sasaki, T., Hosokawa, T., Takada, S.: Phys. Scr. **39**, 655–7 (1989)
7. Yamasaki, T., Ogino, Y., Honda, T., Amemiya, Y.: Scr. Metall. **23**, 1963–8 (1989)
8. Niu, Y.C., Bian, X.F., Wang, W.M.: J. Non-Cryst. Solids **341**, 40–45 (2004)
9. Li, G., Jiang, M.Q., Jiang, F., He, L., Sun, J.: Appl. Phys. Lett. **102**, 171901 (4pp) (2013)
10. Li, J.M., Quan, M.X., Hu, Z.Q.: J. Mater. Sci. Tech. **13**, 61–4 (1997)
11. Cabral-Prieto, A., Garcia-Santibáñez, F., López, A., López-Castañares, R., Olea Cardoso, O.: Hyperfine Interact **161**, 69–81 (2005)
12. Wu, T.W., Spaepen, F.: Philos. Mag. B **61**, 739–50 (1990)
13. Dubois, J.M., Bastick, M., Le Caër, G., Tete, C.: Revue Phys. Appl. **15**, 1103–11 (1980)
14. Randrianantoandro, N., Greneche, J.M., Varret, F.: J. Magn. Magn. Mater. **117**, 93–101 (1992)
15. Falk, M.L., Langer, J.S.: Phys. Rev. E **57**, 7192–7205 (1998)
16. Raghavan, R., Murali, P., Ramamurty, U.: Acta Mater. **57**, 3332–40 (2009)
17. Falk, M.L., Langer, J.S.: Ann. Rev. Condensed Matter Phys. **2**, 353–73 (2011)
18. Rycroft, C.H., Bouchbinder, E.: Phys. Rev. Lett. **109**, 194301 (5pp) (2012)
19. Le Caër, G., Dubois, J.M.: J. Phys. E Sci. Instrum. **12**, 1083–90 (1979)
20. Jen, S.U., Lee, C.Y.: J. Magn. Magn. Mater. **89**, 214–20 (1990)
21. Dubois, J.M., Le Caër, G.: J. de Phys. **C9**, 67–74 (1982)
22. Škorvánek, I., Zentko, A., Miglierini, M., Kováč, J.: Hyperfine Interact **59**, 301–4 (1990)
23. Greneche, J.M., Henry, M., Varret, F.: J. Magn. Magn. Mater. **26**, 153–6 (1982)
24. Bourrous, M., Varret, F.: J. Magn. Magn. Mater. **66**, 229–35 (1987)
25. Barandiarán, J.M., Hernando, A.: J. Magn. Magn. Mater. **104–107**, 73–6 (1992)